

# Laser Communication System Design for the Google Lunar X-Prize

Sreeja Nag<sup>1</sup>, Edwin Gomez<sup>1</sup>, Sam Feller<sup>2</sup>, Jonathan Gibbs<sup>1</sup>, Jeffrey Hoffman<sup>1</sup>

<sup>1</sup>Massachusetts Institute of Technology, Cambridge, MA02139

Phone: 617-710-1845, Email: [sreeja\\_n@mit.edu](mailto:sreeja_n@mit.edu)

<sup>2</sup>Lincoln Laboratory, Lexington, MA 02420

*Abstract*—Laser communications systems offer a significant advantage over traditional radio frequency systems due to the shorter wavelength of laser light. Data can be sent at higher rates for less power with proportionally smaller transmitters and receivers. A laser communications system has never been demonstrated in a moon to Earth link at MBps data rates. This paper presents a model of a laser downlink from the moon, developed to rapidly explore various system architectures. Modeling and analysis shows that the target data rates of above 2 Mb/s are possible with 300mW of transmitter power using a 3.5 mm aperture, a 1.5 m receiver diameter and a minimum gimbal resolution (maximum step size) of 78  $\mu$ rad. 19.89 Mb/s data rates are possible using a 1 cm transmit aperture but with a much stricter minimum gimbal resolution (maximum step size) of 27  $\mu$ rad.<sup>12</sup>

## TABLE OF CONTENTS

1	INTRODUCTION.....	1
2	METHODOLOGY.....	1
3	MODEL RESULTS .....	16
4	CONCLUSIONS.....	19
5	ACKNOWLEDGEMENTS .....	19
6	REFERENCES.....	19
7	BIOGRAPHY .....	20

## 1 INTRODUCTION

Lincoln Laboratory is interested in developing a laser communications system for use on an MIT spacecraft competing in the Google Lunar X-Prize (GLXP). The Google Lunar X-Prize is a competition to land a rover on the moon, take video, traverse a short distance, take more video, and transmit it back to Earth. It would not be the primary means of communication between the lander and Earth, but would allow Lincoln to demonstrate its laser communication technology in a downlink from the lander to Earth. Although laser communications systems have been demonstrated in ground to ground links, and ground to satellite links and vice versa, they have not been demonstrated in links from the moon at data rates greater than 2 MBps. Laser communications systems' chief advantage over radio frequency systems is due to the shorter wavelength of laser light. First, the higher frequency allows

higher modulation rates, and hence more data to be transmitted. Second, because the diffraction limit and the ability to direct a beam is related to the wavelength of light  $\lambda$  and the diameter of the transmitter aperture  $D$  by  $\lambda/D$ , for the same aperture, light can be directed in a beam that is orders of magnitude narrower than RF. This means that data can be sent at much higher data rates for much less power than RF, with the chief downside being the need to direct the beam with great accuracy.

The goal of this project is to develop the system specifications for a laser communications system from the moon to Earth. The key free variables to explore are beam width, pointing accuracy, transmitted power, receiver diameter, background filtering, and modulation scheme. Other factors which will be critical to the performance of the system include orbital geometry, lunar background, gimbal pointing errors, laser stability, and atmospheric losses.

## 2 METHODOLOGY

The methodology used to develop system specifications for a laser communications downlink was to build a system model using STK and Matlab to allow rapid exploration of tradespaces and determine impact of changing several variables at once on system performance. The key independent variables in the system tradespace include transmitter diameter, receiver diameter, receiver field of view, transmitted power, and modulation scheme. The key dependent variables, which are the system performance metrics, include power received, signal to noise ratio, and data rate. A systems level diagram describing how each of the critical variables (independent and dependent) interact with each other to produce the final data rate starting from the power transmitted by the laser is shown in Figure 1.

### Overview

*STK*—STK is a commercial simulation that models the interaction between spacecraft, planets, and planetary bodies in deep space. The simulation is being used to generate a set of environmental variables that will bind the environment in which the system will operate. These variables include lunar phase angles, pointing vector, signal distance, and times where there is a line of sight between the possible laser receiver locations and the moon.

<sup>1</sup> 978-1-4244-7351-9/11/\$26.00 ©2011 IEEE

<sup>2</sup> IEEEAC paper#1683, Version 3, Updated 2011:02:02

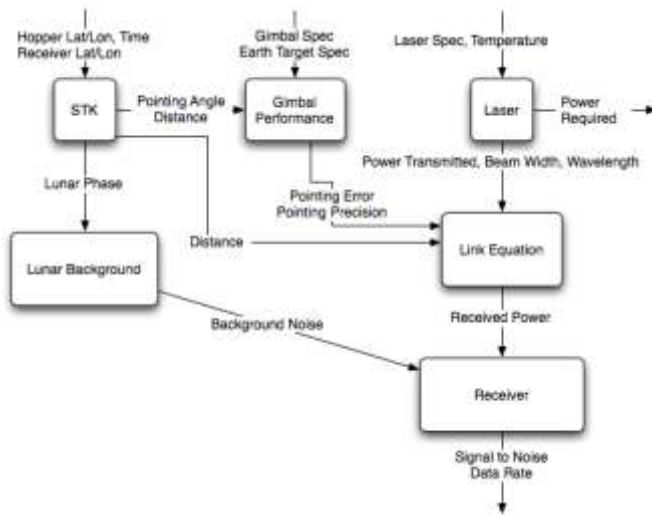


**Figure 1 – System Diagram**

*Laser System*—The Laser component of the system is responsible for transmitting the signal to the Earth with enough power to achieve the overall system performance goal of 1-2Mb/s. Transmitting a signal successfully is a requirement to win the Google Lunar X-prize and transmitting the signal with a high data rate to validate the high data rate capabilities of deep space optical communications.

The key laser design variables are input power, desired wavelength, beam width, and modulation type. The key performance variables are power transmitted, power required, and wavelength error. Additionally, the performance of the laser is highly dependent upon the temperature surrounding it so the cooling system performance is critical and highly coupled to the laser performance. The temperature specifically affects the wavelength error on the order of .05nm per degree C difference nominal temperature, and the gain which drives the amount of power that is actually transmitted.

The actual laser design and performance characteristics are classified as Lincoln Laboratory proprietary material so a mathematical model of the Laser sub system will not be included in this study. Instead, the following values from Table 1 are assumed:

Variable	Value
Power Transmitted	300 mW
Wavelength (nominal)	1064nm
Wavelength error	<1 nm

**Table 1 - Laser Parameters**

*Link Equation*—The link equation represents an estimation of the total power losses that occur over the distance of the signal transmission. There are both power losses and gains. There is also a pointing loss from the gimbal which is treated as a performance variable of the gimbal system.

*Lunar Background*—The lunar surface reflects sunlight to the earth along the same vector as the laser signal causing an increase in background noise, an environmental variable. The lunar background is primarily dependent upon wavelength and the lunar phase angle. The lunar background module takes a lunar phase angle from the STK module and sends the lunar flux level to the receiver module.

*Receiver*—The receiver’s function is to receive the signal for the laser and convert the signal into binary data at a data rate that is as high as possible. There are currently three receiver sites and two types of pointing methods (for the hopper to locate the receiver) under consideration. There are two design variables that can be varied to accommodate the anticipated signal strength, and wavelength: the receiver field of view and the receiver diameter.

*Gimbal*—The gimbal system is responsible for accurately pointing the laser at the receiver on the Earth. For each type of gimbal, there will be a minimum step size resolution in the equipment specification. This step size can be thought of as a design variable but can only be changed discretely by switching gimbals.

*Space Mission Geometry*

The Earth’s, Sun’s and Moon’s center were chosen as the coordinate system centers for orbit analysis and geometry on the Earth and Moon surfaces. The Space Mission Geometry (using STK) and Pointing Mechanisms will provide valuable information to determine line of sight between the laser device (on the Moon) and the laser receiver (on the Earth), as well as data to calculate the Background Noise and the Laser Link Equation (see **Error! Reference source not found.** and Figure 3).

*Earth geometry viewed from space*—The most common problem in space mission geometry is to determine the relative geometry of objects on the Earth’s surface as seen from the Moon. One example is to use the given coordinates of a target (receiver) on the Earth to determine its coordinates in the Moon field of view. Another is to determine the intercept point on the surface of the Earth corresponding to a given direction in laser device coordinates. To begin, the angular radius of the spherical Earth as seen from the laser device on the Moon ( $\rho$ ) and the angular radius measured at the center of the Earth of the region seen by the laser device ( $\lambda_o$ ) should be determined. Because it has been assumed a spherical Earth, the line from the laser device to the Earth’s horizon is perpendicular to the Earth’s radius, and therefore:

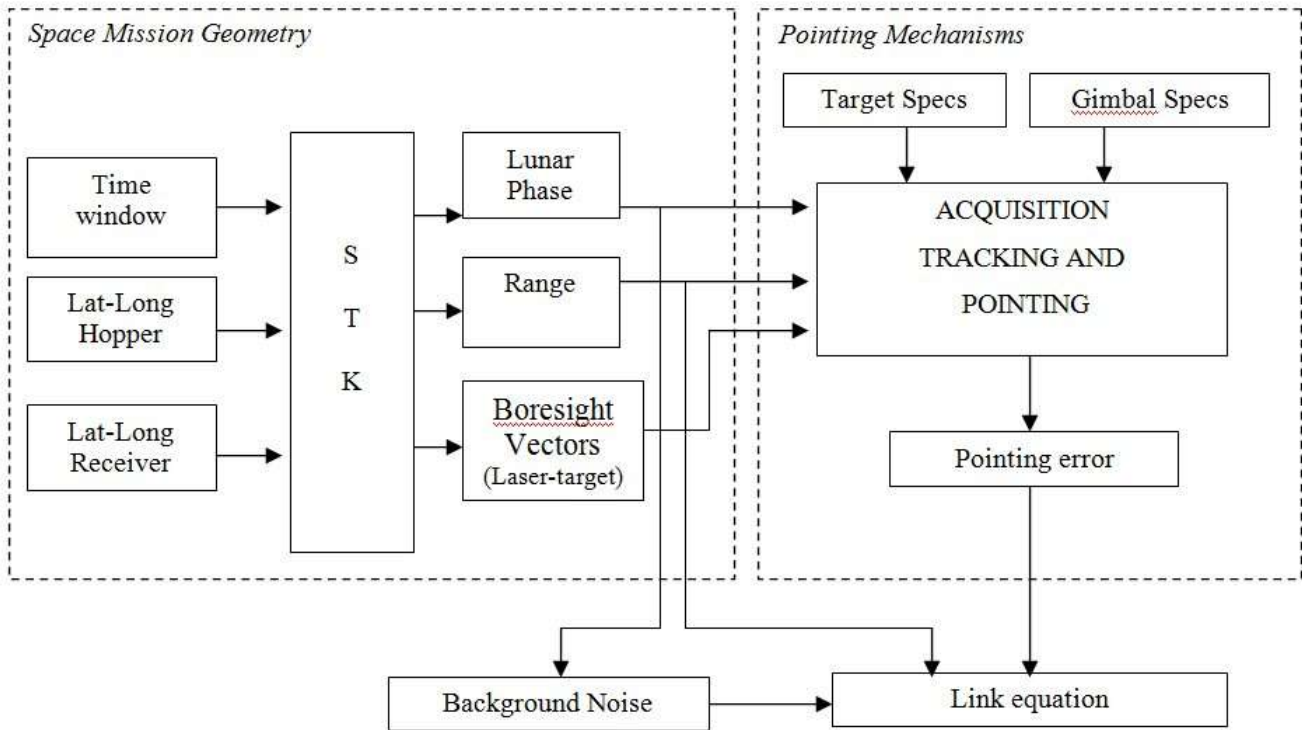


**Figure 2: Space Mission Geometry and Pointing Mechanisms Block Diagram**

$$\sin \rho = \cos \delta = R_E / (R_E + H) \quad (1)$$

$$\rho + \delta = 90 \text{ (degrees)} \quad (2)$$

$$S = 2 \pi R_E^2 (1 - \cos \delta) \quad (3)$$

Where  $R_E$  is the radius of the Earth,  $H$  is the altitude of the laser device, and  $S$  is the surface area visible[1] from the laser device. Thus, the Earth forms a small circle of radius  $\rho$  on the laser device sky, and the laser device sees the area within a small circle of radius  $\delta$  on the surface of the Earth. The distance,  $D_{\max}$ , to the horizon is given by:

$$D_{\max} = [(R_E + H)^2 - R_E^2]^{1/2} = R_E \tan \delta \quad (4)$$

The spherical-Earth approximation is adequate for most mission geometry applications. From the Moon, the Earth appears somewhat round rather than oblate, so it is not needed to apply a correction for Earth's oblateness and spherical coordinates both on the Earth and on the Moon will be used for computations. The maximum latitude and the percentage of the Earth's surface visible from the laser device can be calculated using equations described above ( $R_E = 6,378.13649$  km,  $H_{\text{perigee}} = 354,988.76351$  km,  $H_{\text{apogee}} = 397,580.76351$  km).

a) Using the perigee altitude ( $H_{\text{perigee}}$ )

$$\cos \delta = R_E / (R_E + H)$$

$$\cos \delta = 6,378.13649 / (6,378.13649 + 354,988.76351)$$

$$\delta = \cos^{-1}(0.01765002962)$$

$$\delta = 88.988675^\circ$$

$$\rho = 90 - \delta$$

$$\rho = 90 - 88.988675$$

$$\rho = 1.0113247^\circ$$

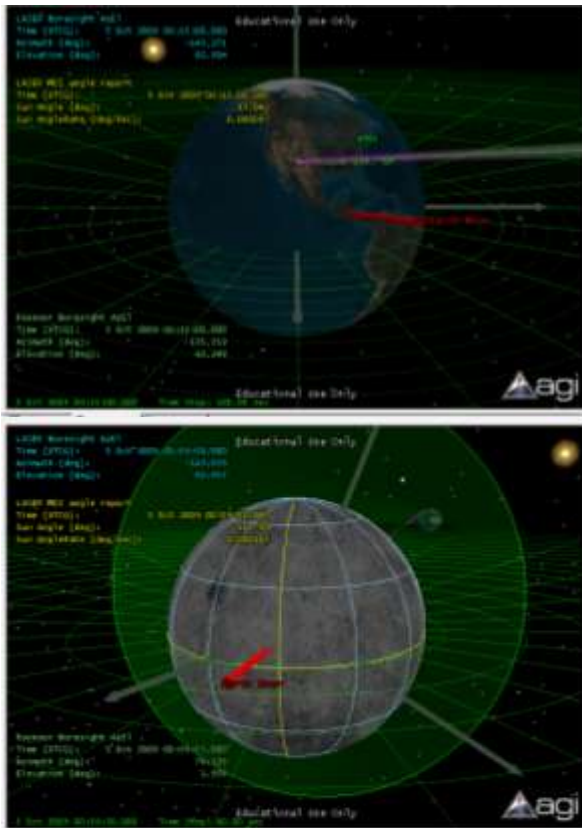


**Figure 3 Earth and Moon view using STK**

$$S = 2 \pi R_E^2 (1 - \cos \delta)$$

$$S = 2 \pi (6,378.13649)^2 (1 - 0.01765002962)$$

$$S = 251,092,488.058021 \text{ km}^2$$

Therefore, the percentage of the hemisphere visible from the laser device on the Moon is:

$$S/2\pi R_E^2 * 100 = (1 - \cos 88.988675^\circ) * 100 = 98.234996\%$$

b) Using the apogee altitude ( $H_{\text{apogee}}$ )

$$\delta = 89.095315^\circ$$

$$\rho = 0.904685^\circ$$

$$S = 251,568,157.138279 \text{ km}^2$$

$$S/2\pi R_E^2 * 100 = (1 - \cos 88.988675^\circ) * 100 = 98.421093\%$$

Next it is required to find the relationship between the nadir angle ( $\eta$ ) measured at the laser device from the subsatellite point (*nadir*) to the target (receiver); the Earth central angle ( $\lambda$ ), measured at the center of the Earth from the subsatellite point to the target; and the grazing angle or laser device elevation angle ( $\varepsilon$ ), measured at the target between the laser device and the local horizontal (see Figure 4).

The angular radius of the Earth can be calculated with Equation 1. Next, if  $\text{vis}$  is known,  $\eta$  can be found from:

$$\tan \eta = \sin \rho \sin v / (1 - \sin \rho \cos \lambda) \quad (5)$$

If  $\eta$  is known,  $\varepsilon$  can be found from:

$$\cos \varepsilon = \sin \eta / \sin \rho \quad (6)$$

Or, if  $\varepsilon$  is known,  $\eta$  can be found from:

$$\sin \eta = \cos \varepsilon \sin \rho \quad (7)$$

The remaining angle and side are obtained from:

$$\eta + v + \varepsilon = 90 \text{ (degrees)} \quad (8)$$

$$D_{LT} = R_E (\sin v / \sin \eta) \quad (9)$$

Where  $D_{LT}$  is the distance between the laser device on the Moon and the laser receiver on the Earth. If the latitude and longitude of the Hopper (where the laser device is mounted) on the Moon, the Receiver on the Earth and the time

window of operation are known, the STK model calculates the dates and times when the laser payload has line of sight with the receiver (see red areas on Figure 5).

**Lunar Phase Angle ( $\theta$ )**—The same analogy described on Figure 4 is used to find the Lunar Phase Angle ( $\theta$ ) which is required to determine the lunar reflectance ( $A_K$ ) in order to calculate the Lunar Irradiance ( $I_K = A_K \Omega_M E / \pi$ ) which is going to be addressed in detail in the background noise determination.

$$\sin \rho = \frac{r_2}{r}$$

$$\cos \varepsilon = \frac{\sin \eta}{\sin \rho}$$

$$r_2 = R_E + R_M + D_{LT} \quad \eta + v + \varepsilon = 90$$

$$r_1 = r_2 \left( \frac{\sin v}{\sin \eta} \right) \quad \theta = 90 + \varepsilon$$

Where  $r$  is the distance Sun to Earth,  $r_1$  is the distance Sun to Moon, and  $r_2$  is the distance Moon to Earth (all center to center), and  $D_{LT}$  is the distance laser device on the moon to laser receiver on the Earth. [ $R_M = 1,378.14 \text{ km}$ ] (See Figure 6)

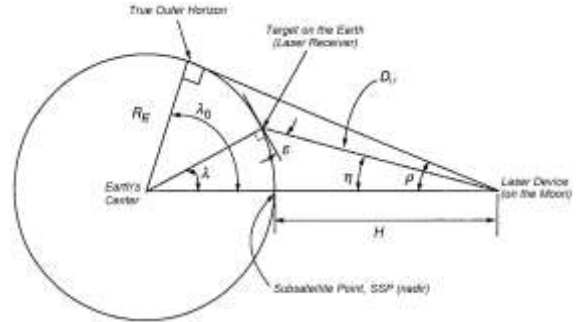


**Figure 4 – Definition of Angular Relationship between Laser Device (on Moon), Target (Receiver on Earth), and Earth Center**

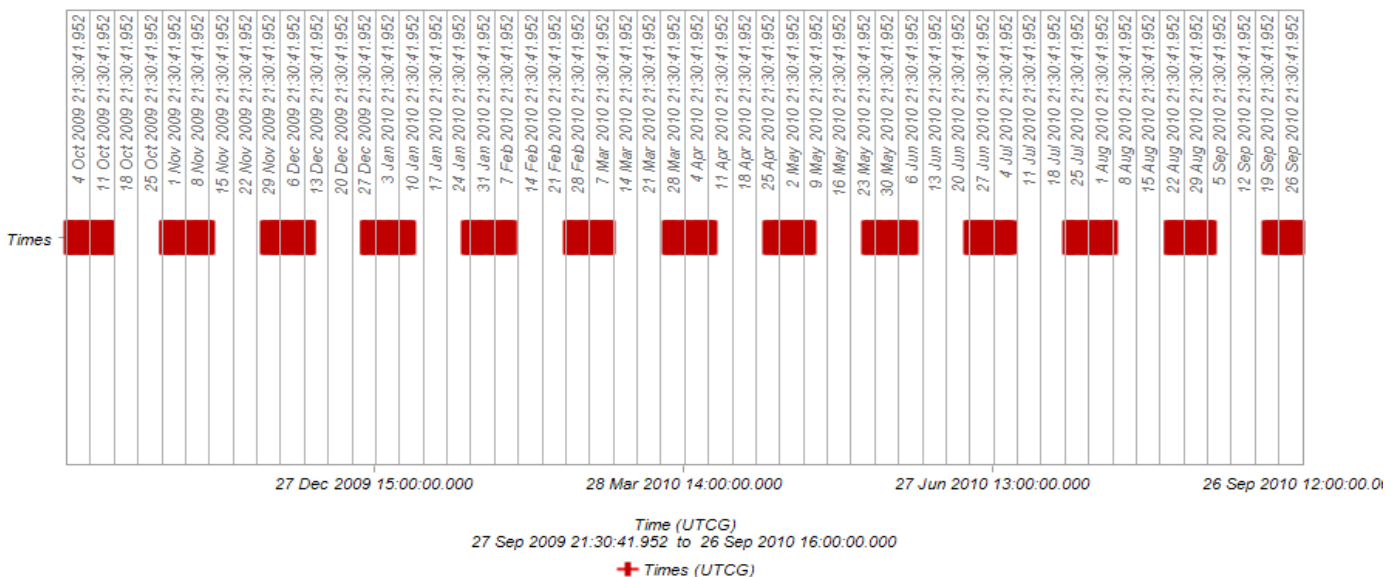


**Figure 5 – Dates and times when the laser device on the Moon has sight line with the laser receiver on the Earth from 27 Sep 2009 16:00:00.000 UT CG to 26 Sep 2010 16:00:00 UT CG**

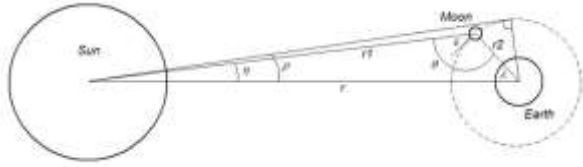


**Figure 6 – Definition of the Lunar Phase Angle between Laser Device (on the Moon), Target (Receiver on Earth) and Sun Center.**

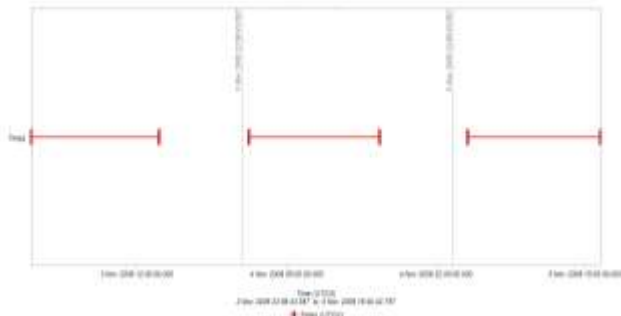


**Figure 7 – Target Access Time Report from 2 Nov 2009 to 5 Nov 2009**

Target Access Times (TAT) indicates the total time window when the laser payload on the Moon has sight line with the laser receiver on Earth (see Figure 7), so: 1<sup>st</sup> TAT = 14.5 hours, 2<sup>nd</sup> TAT = 14.9 hours, and 3<sup>rd</sup> TAT = 15.1 hours. Considering the Target Access Time, Range and Lunar Phase, the optimal time to transmit the laser beam can be determined. The Lunar Phase variations are: 1<sup>st</sup> TAT = 5.04 to 10.196 (deg), 2<sup>nd</sup> TAT = 16.37 to 23.216 (deg), and 3<sup>rd</sup> TAT = 30.120 to 36.839 (deg). This information indicates how much lunar reflectance variation can affect to the background noise (see Figure 8).

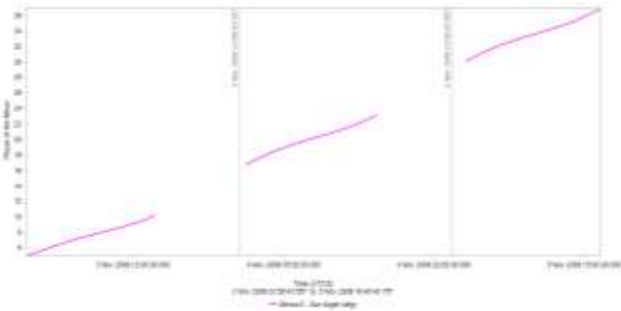


**Figure 8 – Lunar Phase Angle from 2 Nov 2009 to 5 Nov 2009**

*Range and Boresight Vector* —Space loss is the highest loss that directly affect the Received Power on the Earth; for this reason, it is very important determine the range when the laser device and the laser receiver are closer, as well as the boresight vector in azimuth and elevation. Figure 9 shows that the minimum range is 362,382.515310 km with Az=

212.074 (deg) and El= 85.449 (deg) on 5 Nov 2009 09:21:42.251

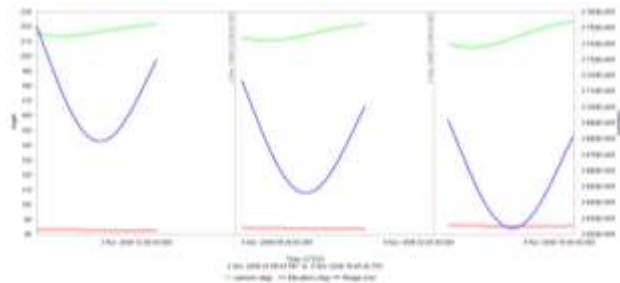


**Figure 9 – Range and Boresight vector Laser Device to Laser Receiver from 2 Nov 2009 to 5 Nov 2009**

*Link Equation*

Power transmitted on the moon is scaled down by a transfer function of propagation to give power received on Earth. The exact representation of the wave propagation model is by calculating intensity at a distance from the source and integrating over the surface area considered in order to get power. In the following results of the link equation the relationships between the average power transmitted at the source, modeled as a Gaussian, and average power received at the target (at the (0,0) position of the image plane) i.e. the maximum average power received are considered. The fall in power at off-axis points will be discussed later in relevance to pointing requirements of the laser beam. This process is given by the link equation [2]:

$$p_0 = p_t \cdot G_t \cdot G_r \cdot S \cdot E_p \cdot A_{tm} \quad (10)$$

Where  $p_0$  = power that reached earth,  $P_t$  = power transmitted on the moon,  $G_t$  = Transmitter Gain,  $S$  = Space propagation losses,  $E_p$  = Pointing error of the pointing and tracking system,  $A_{tm}$  = Atmospheric losses. Thus the scaling transfer function is  $T_f = G_t \cdot G_r \cdot S \cdot E_p \cdot A_{tm}$  [3]. Losses also occur due to less receiver sensitivity and receiver dark currents and other noise terms and they are treated as background and dealt with in signal to noise ratios. In this equation, transmitter gain is given by,

$$G_t = \frac{16}{a^2} \quad (11)$$

$$\theta_T = \frac{2\lambda}{\pi w_0} \quad w_0(\max) = \frac{Dt}{2} \quad (12)$$

Where  $\theta_T$  is the linear approximation of the beam divergent angle of a Gaussian beam with initial beam waist (diffraction limited for the purpose of this discussion) of  $w_0$  releasing wavelength of light  $\lambda$ .  $w_0$  can be a maximum of half the aperture diameter of the transmitter. Similarly space losses and receiver gain is given by,

$$S = \left(\frac{\lambda}{4\pi L}\right)^2 \quad G_r = \left(\frac{\pi D}{\lambda}\right)^2 \quad (13)$$

Where  $D$  = receiver aperture diameter,  $L$  = propagation path distance which here is the distance between transmitter on moon and receiver on earth.

*Beam Spread Losses*—The transmitter and receiver losses together with the space losses give a term called beam spread losses [4] which is

$$\frac{D_r^2}{beam\_diam^2} \quad (14)$$

Where  $beam\_diam$  is the diameter of the laser beam on the earth given by:

$$beam\_diam = \frac{4\lambda L}{\pi D_t} \quad (15)$$

For transfer functions, its various components are usually expressed in decibels so that the contribution of each can be noted individually and the total contribution can be seen as a sum of their parts. Since Loss in decibels =  $10\log_{10}$  (Factor in ratios) so given from the equation above, Beam spread loss =  $20\log D_r - 20\log(beam\_diam)$ . From Figure 10 – Tradespace of the Diameter of Laser Spot on Earth, it is easy to note that the beam diameter falls off with distance as an inverse square curve, hence the larger the aperture, the lesser the beam spread and more the energy transferred to the Earth within a short range. Given the finite size of the receiver, the smaller the beam divergence, more the energy it will capture. Although the earth-moon distance changes with time, the corresponding change is not very large in the beam diameter – about 20 km, which is about 1dB of difference in transfer function losses – as shown in Figure 10. For  $D_r = 3.5m$ ,  $L = 378000km$ ,  $\lambda = 1064nm$ ,  $D_t = 5cm$ , the beam spread Loss is -138 dB – which is the highest among all other losses. The apogee-perigee variation seems to be very less compared to this but is comparable to atmospheric losses.

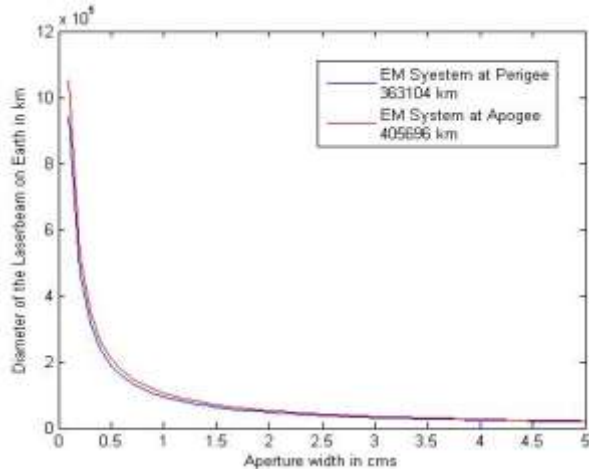


**Figure 10 – Tradespace of the Diameter of Laser Spot on Earth**

*Atmospheric Losses*—The availability of a clear sky is very important for the laser link to be established, thus transmission happens only at night for about 6-12 hours. The atmosphere causes a dual effect – one, it absorbs the

light and releases it later as heat i.e. simple attenuation. Two, it causes background sky radiance that adds to noise due to molecular or Rayleigh scattering and Aerosol or Mie scattering. Both are heavily influenced by the wavelength of propagating light. The atmospheric loss module comprises the following components:

- Simple attenuation
- Scintillation effects (Optical Turbulence, Beam Wander, Atmospheric Jitter)
- Fried Parameter representation

*Simple attenuation*—Simple attenuation [5] depends on visibility or density (fog, near fog and clear) of atmosphere and is effective only after beam enters atmosphere (last ~ 10 km of its ~ 378000 km journey. Again, 60% of the atmosphere is concentrated in the last 5 km).

$$\tau(L) = \frac{P(L)}{P(0)} = e^{-\sigma L} \quad (16)$$

Where  $\zeta$  is atmospheric transmittance,  $P(L)$  is the laser power at  $L$ ,  $P(0)$  is the laser power at the start and  $\sigma$  is the attenuation or extinction coefficient per unit length given by:

$$\sigma = \frac{3.91}{V} \sec(\eta) \left(\frac{\lambda}{550nm}\right)^{-q} \quad (17)$$

Where  $V$  = visibility of the atmosphere in kms,  $\eta$  is the zenith angle,  $q$  = scattering distribution of particles.

Although the height of the atmosphere is 11 km, 90% of its content is located in the first 6km – the height of the highest clouds (Cirrus series). The difference between fog and clouds is essentially the height at which the moisture condenses – below 100 feet for fog and above that for clouds. It is thus useful to note that the transmittance thus depends on the zenith angle, visibility due to clouds/fog and the height to which this visibility extends. Heavy fogs have 2-5 km visibilities, lighter fogs have up to 20 km visibility and clear skies greater than 20 km. The assumption is that the laser communication will be initiated only when the skies are relatively clear, hence the loss due to the atmosphere will not be much. Figure 11 thus shows the loss in decibels due to simple attenuation for an optimistic visibility of 15 to 23 km. The loss is clearly more as this condition extends higher into the atmosphere. The atmospheric effects do not depend on the apogee-perigee distance as their effect extends only in the last 11 km of the laser beam propagation. Thus for an optimistic estimate, relatively clear skies with visibility of 20 km and rare clouds that extend up to 3 km give an atmospheric loss of ~ 3 dB. This value has been plugged into the link equation and can be changed subject to the weather conditions at the downlink receiver station.

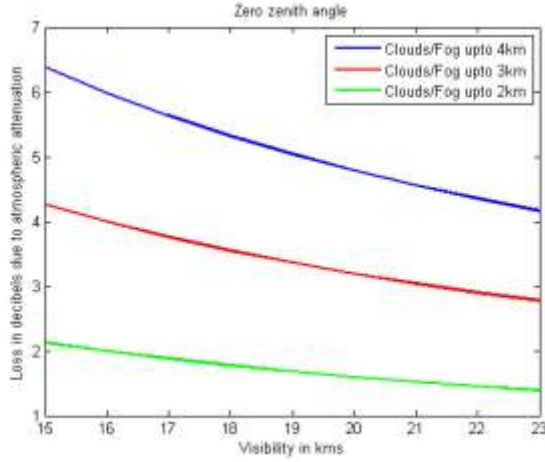


**Figure 11 – Atmospheric Transmittance Loss**

**Scintillation**—In the absence of turbulence, a Gaussian beam is broadened by diffraction and has, in the far field, a beam radius as discussed before. When analyzing the beam radius in a turbulent medium, the situation is more complex, and it is usually necessary to distinguish between the short-term and the long-term beam spread. Generally speaking, when a finite optical beam interacts with refractive index inhomogeneities due to atmospheric turbulence, it is found that those turbulent eddies which are large compared to the diameter of the beam tend to deflect the beam, whereas those eddies that are small compared with the beam diameter tend to broaden the beam, but do not deflect it significantly. Consequently, if one observed the laser spot on a screen in the plane of the receiver aperture, and took a very short exposure picture, one would observe a laser spot which is broadened to  $w_{st}$  (due to the small eddies) and is deflected by some distance to  $r_{bw}$  from the optical axis in an effect called beam wander or beam steering – as seen in Figure 12.

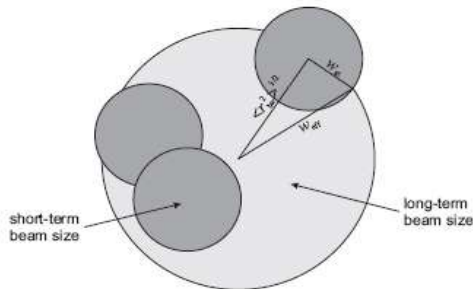


**Figure 12 – Beam scintillation graphic**

Fluctuations in the received intensity resulting from propagation through atmospheric turbulence are commonly referred to as scintillation. A well-known manifestation of this phenomenon is the twinkling of stars. Due to its effects, the intensity over the receiver aperture is not uniformly distributed leading to scintillation losses quantified by the Scintillation index. This depends on Strength of turbulence or the effective refractive index of the atmosphere ( $C_n$ s), wavenumber, length travelled, transmitter aperture, receiver diameter, collinearity of beam (assumed=1), coherency of

beam (assumed=1). Mathematically, aperture averaging scales the scintillation index by a factor of  $A$  because the traditional scintillation index assumes that the lens diameter aperture is zero. Scintillation index is given by [6,7]:

$$\sigma_I^2(r, L) = \frac{\langle I_{det}^2(r, L) \rangle}{\langle I_{det}(r, L) \rangle^2} - 1 \quad (18)$$

Here the  $I(r, L)$  is the intensity at the radial position of  $r$  at the range of  $L$  from the laser source. Power over the receiver plane (also assumed to be a Gaussian) is obtained by integration:

$$\int_{-\infty}^{\infty} \int_{-\infty}^{\infty} I(x, y, z) dx dy = |B|^2 \int_0^{2\pi} d\theta \int_0^{\infty} \frac{\rho^2 \cos^2 \theta + z^2}{(\rho^2 + z^2)^2} \exp\left(-\frac{2}{C^2} \frac{\rho^2}{\rho^2 + z^2}\right) \rho d\rho \quad (19)$$

The approach used is described as follows:

**CALCULATE CNS:** [8] The other precise options to calculate were location specific and required turbulence length and wind speed velocity hence instead, a standard one was used. The 50% median case is assumed for the calculations from Table 2. The atmosphere is assumed to be up to a height of 4 km.

$$C_n^2(h) = c_1 + c_2 \exp(-h/c_3) + c_4 \exp(-h/c_5), \text{ for } 0 \leq h \leq 6000 \text{m} \quad (20)$$

Any of the three given cases can be assumed depending on the weather conditions at the downlink receiver station, however for modeling purposes the best case is used; for example, assuming that downlink will initiate only when clear skies are available.

Case & Percentile	$C_n^2(h=0)$ ( $m^{-20}$ )	$c_1$ ( $m^{-20}$ )	$c_2$ ( $m^{-20}$ )	$c_3$ (m)	$c_4$ ( $m^{-20}$ )	$c_5$ (m)
"Best" - 10%	1.0E-16	9.8286E-18	7.1609E-17	100	1.9521E-17	1500
Median - 50%	8.0E-16	9.8583E-18	4.9877E-16	300	2.9228E-16	1200
"Worst" - 10%	1.0E-14	9.2002E-18	9.4387E-15	800	6.7328E-16	1000

**Table 2 – Maritime constants**

**CALCULATE RYTOV COEFFICIENT:** This is also known as the scintillation index. As cited, the beam-propagation simulation reported indicates as much as a 10-fold reduction for Rytov variances between 0.4 and 0.5 and a 3-fold to 4-fold reduction for Rytov variance close to 0.2.

The value is calculated as follows [9]:

$$\theta = 1.23 CNS k^{7/6} L^{11/6} \quad (21)$$

In the example, as the beam enters the atmosphere and propagates downward, the length of the downlink propagation path increases. Under weak turbulence

conditions, the index grows linearly with CNS until it reaches a maximum value because the focusing caused by large-scale inhomogeneities achieves the strongest effect. With increasing path length the focusing effect is weakened and the fluctuations begin to decrease, – shown in Figure 13. The variance is well below the 0.2 – the benchmark for modeling-significant turbulences of according to the geostationary Earth orbit (GEO) laser communications demonstration (GOLD) by JPL.

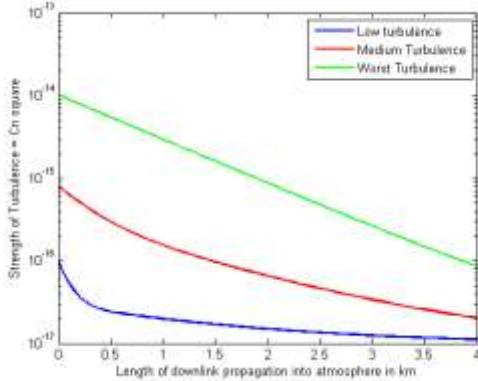


**Figure 13 – Rylov Variance**

**CALCULATE COHERENT LENGTH:** This indicates the transverse direction in which the electric field is coherent and is calculated as [10]:

$$\rho_{sp} = \left( 2.9k^2 CNS * L * \frac{3}{8} \right)^{-3/5} \quad (22)$$

**CALCULATE EFFECTIVE RADIUS by:**

$$w_{\text{eff}} = \frac{\lambda L}{\pi w_0} \sqrt{1 + \left( \frac{w_0}{\rho_{sp}} \right)^2} \quad (23)$$

Since the order of the laser spot on Earth is about 60-100 km, the change due to the coherence diameter in the order of 10s of meters (as the coherence diameter is calculated out to be) does not make much of a difference and are ignored in the modeling calculations.

Strength of turbulence	1.1185e-017
Scintillation index	0.0044
Short term beam diameter	51.48 kilometers
Coherent length (radius)	1.09 meters
Aperture averaging factor	0.0086

**Table 3 – Results for atmospheric transmission factors in downlink Laser Communication**

Since the scintillation factor does not change much with diameter, the results of the assumed optimistic case are

presented in Table 3 for Earth Moon distance of 380000 km, 4000m atmosphere, best case condition in the Maritime model, Transmitter diameter = 1 cm, Receiver diameter = 3.5m and coherent, collimated, Gaussian beam. Clearly then, the Beam Wander is negligible for the size of the laser spot considered for downlink in cases of clear weather conditions.

**Turbulence**—A quantity often used for the characterization of the strength of atmospheric turbulence, especially in connection with astronomical imaging, is the Fried parameter  $r_0$ . It is another form of the atmospheric coherence length and is given by:

$$r_0 = \left[ 0.423k^2 \int_{Path} C_n^2(s) ds \right]^{-3/5} = [0.423k^2 C_n^2 L]^{-3/5} \quad (25)$$

The image of a point source, like a star, in an ideal telescope without atmosphere depends solely on diffraction and is described by an Airy function. Since the first dark ring appears at an angular distance of  $1.22\lambda/D$  from the center, the ratio  $\lambda/D$  equals roughly the angular extent (seeing angle  $\beta$ ) of the star image, and is often taken as a measure for the resolution of an ideal telescope. Under the influence of atmospheric turbulence, the seeing angle is limited by  $\beta = 0.98\lambda/r_0$ . This value comes out to 171 cm in the assumed case (height of atmosphere 2km, best Maritime model case). A more mathematical formulation of transmission is given for the White Sands region [11] in New Mexico and is given by:

$$MTF(f) = \exp \left[ -3.44 \left( \frac{\lambda R f}{r_0} \right)^{5/3} \right] \quad (25)$$

Where MTF = Long-term atmospheric modulation transfer function,  $f$  = Spatial frequency of image plane (assumed  $13e-6$  m is the size of the detector pixel on the APD array of Lincoln Labs) [12],  $R$  = Focal length of receiving system. The experimental results of  $r_0$  are represented in Figure 14 [13]. This shows that the assumed conditions overestimate the quality of transmission because the seeing angle would be 5 times less (power received thus more) than that which is experimentally measured. However, it could be argued that transmission is planned to occur only in very clear skies, not all times as the New Mexico experiments measure. Keeping some leeway, nonetheless, the atmospheric loss is assumed to -6 dB (for all atmospheric components) for further modeling in this paper.

*Background Noise*

The sensitivity of the Geiger-Mode Avalanche Photo Diodes to levels as low as a single photon means that the impact of any background noise can be significant and must be characterized. In this section, the approach to modeling background noise is described by:

$$N = \Sigma B * FOV * F \quad (27)$$

Where N is the total background noise in Watts,  $\Sigma B$  is the sum of all noise sources, in  $W/(m^2 * sr)$ , FOV is the solid angle visible at the receiver, and F are filtering losses.

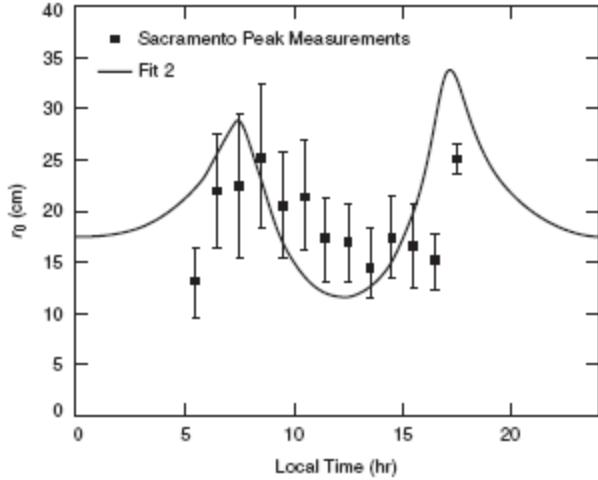


**Figure 14 – Daily variation of atmospheric coherence length, experimentally measured at New Mexico**

*Background Sources*—The Google Lunar X-Prize hopper will transmit from the moon, from the portion of the moon lit by sunlight and not in Earth’s shadow. Hence, the receiver on Earth will have line of sight access to the moon during the night time. The two largest sources of background noise will be Lunar radiance and sky radiance. Because Lunar radiance dominates, sky radiance has been neglected for this model. Lunar radiance was modeled using information taken from the Robotic Lunar Observatory (ROLO) [14], which is sponsored by the U.S. Geodetic Survey. The ROLO project has carefully measure Lunar reflectance across a range of wavelengths for purposes of providing a consistent calibration source for on orbit satellites.

The ROLO model gives reflectance  $A_k$  at wavelength  $k$  as a function of phase angle of the moon  $g$ , selenographic longitude of the sun  $\Phi$ , and selenographic latitude and longitude  $\theta$  and  $\phi$ , as well as several empirically determined coefficients that vary with wavelength as

$$\ln A_k = \sum_{i=0} a_{ik} g^i + \sum_{j=1} b_{jk} \Phi^{2j-1} + c_1 \theta + c_2 \phi + c_3 \Phi \theta + c_4 \Phi \phi + d_{1k} e^{-g/p_1} + d_{2k} e^{-g/p_2} + d_{3k} \cos[(g - p_3)/p_4] \quad (28)$$

Reflectance is plotted vs. wavelength in Figure 15 below. The project team’s Matlab code is shown plotted on the left, along with data from ROLO on the right. They match very well, validating the Matlab code.

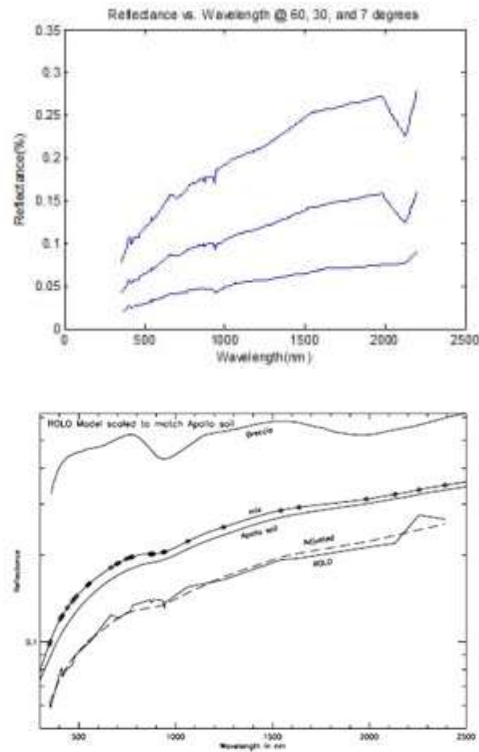


**Figure 15 – Reflectance vs wavelength at lunar phase 60, 30 and 7. It is clearly visible that reflectance decreases with phase.**

Data from the STK model can be used to calculate the lunar phase angle as a function of time. That in turn can be used to calculate the lunar reflectance as a function of time. The reflectance, when combined with the solar flux, can be used to calculate the radiance on earth.

*Receiver Field of View (FOV)* —Received background light varies directly with the FOV of the receiver, and is diffraction limited. Additionally, as the FOV grows smaller, the tracking requirements imposed on the receiver grow more and more stringent. For purposes of this model, receiver FOV is based on previous Lincoln systems and is defined as  $30\mu\text{Rad}$ .

*Filtering*—The laser chosen for the GLXP is very stable in terms of wavelength vs. temperature, less than  $.1 \text{ nm} / ^\circ\text{C}$ . Because of this, it is possible to build a filter with a very narrow band pass to reject as much stray light as possible while still allowing signal light through. As Figure 15 shows, within a narrow range around the 1064nm wavelength, lunar reflectance can be approximated as increasing linearly. Therefore, it follows that background light will increase linearly with the width of the filter. For purposes of this model, the receiver filter is modeled as an ideal band pass filter, 1nm wide.

*Received Background Noise*—A plot of received flux, in  $W/m^2$  is shown below in Figure 16. During a full moon, the flux over a  $30\mu\text{Rad}$  field of view is about  $4e-11 \text{ W}/m^2$ , and falls off at steeper phase angles. Figure 17 shows a plot

using the ROLO model and data generated using STK. Each “track” shows the lunar flux as it varies during each viewing night. The flux peaks once a month when the moon is at its fullest.

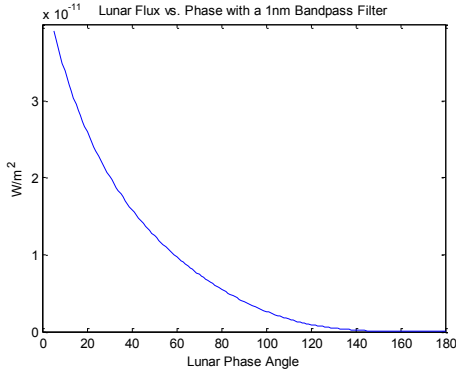


Figure 16

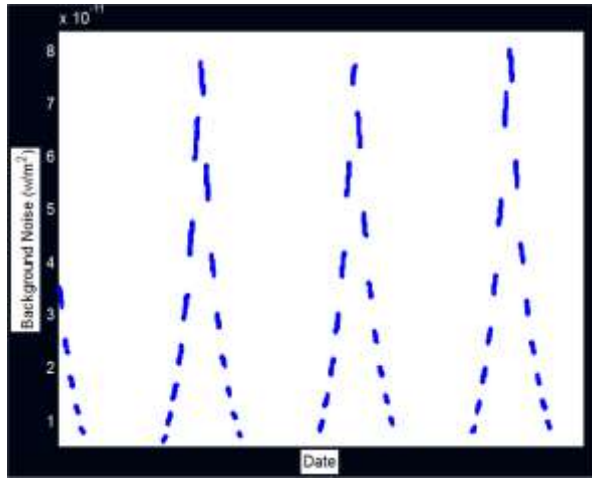


Figure 17 - Lunar Background vs. Viewing Night (1 nm ideal band pass filter, 30µrad FOV). Maximum noise is 8e-11 W/m<sup>2</sup>

Receiver

In this section, the receiver module is described. First, background information on M-ary pulse position modulation and Poisson counting statistics are presented. Next, the equations for converting from signal levels and signal to noise ratios to data rates are presented. Finally, the simplifying assumptions and approximations used to implement the data rate conversion are given.

*M-ary Pulse Position Modulation*—M-ary Pulse position modulation [15] (PPM) is an on-off keyed laser modulation scheme with a duty cycle of 1/M. A given number of time slots are grouped into symbols, with a single laser pulse arriving somewhere within each symbol. Each time slot corresponds to a different word, or set of bits, with log<sub>2</sub>M bits per slot. For example, with 8-ary PPM, as shown in the lower portion of Figure 18, each symbol is comprised of 8 time slots, each slot representing the bits 000, 001, 010, 011, 100, 101, 110, and 111. With M-ary PPM, it is also

important to note the low duty cycle gives the laser a high peak to average power ratio. For example, in situations where there are poor signal to noise ratios, it is possible to increase the modulation order, doubling the M, while also doubling the peak power, and keeping the same average power, thus increasing the signal above the noise floor without any additional power draw on the system.

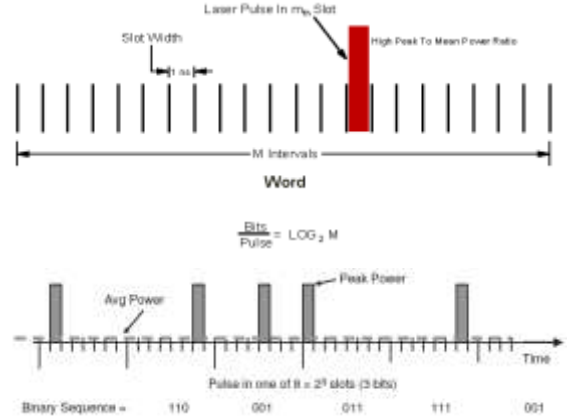


Figure 18: Pulse Position Modulation

*Poisson Counting Statistics*—Laser light, especially at the level of counting single photons, is inherently noisy, and is limited by “shot noise”. Basically, what it means is that if a given number of photons are expected to arrive, on average, in a given time slot, sometime more arrive, sometimes less, sometimes even none. The distribution that it follows is called a Poisson distribution. In a perfect signal channel, for example, with no background noise, the chief source of error would be not counting a photon when a photon was sent. The odds of this happening can be reduced by increasing the average number of expected photons since  $p(k=0) = \exp(-Ns)$ . This can be done by either lengthening the window in which photons can arrive or increasing power to send more photons

*Data Rate Conversion*—Even in a perfect channel with no background noise, the nature of laser light is inherently noisy. Noise is characterized by a Poisson distribution – given an expected rate of photon arrivals, what is the probability of a certain number of photons arriving? The channel capacity as a function of M, and average signal and noise photons per time slot is

$$C_{PPM}(M, n_s, n_b) = \frac{\log_2 M}{M} \left( 1 - \frac{1}{\log_2 M} E_{N_s, \dots, N_b} \log_2 \left[ \sum_{i=1}^M \left( 1 + \frac{n_s}{n_b} \right)^{(N_i - N_1)} \right] \right) \text{ bits/slot} \tag{29}$$

$$N_s = \frac{P_s \lambda T_s M}{hc} \quad N_b = \frac{P_b \lambda T_s}{hc}$$

M = M-ary value for PPM modulation, P<sub>s</sub> and P<sub>b</sub> are signal and noise power respectively, N<sub>s</sub> = signal photons and N<sub>b</sub> = noise photons. The region of low power is noise limited, and higher data rates are achieved by increasing M and hence the peak power. The region with higher power is slot width limited and higher data rates are achieved by reducing M and increasing the duty cycle. Unfortunately, the full

equation for channel capacity is very difficult to implement. The solution is to use two approximations, one for the noise limited region, and one for the slot width limited region, and then to take the minimum of the two (as illustrated in Figure 19).

$$C \leq C_{\text{OOK}} = \frac{1}{\ln 2} \left[ (\lambda_s + \lambda_b / M) \ln \left( 1 + \frac{\lambda_b}{M \lambda_s} \right) + \frac{M-1}{M} \lambda_b \ln \left( 1 + \frac{\lambda_b}{M \lambda_s} \right) - (\lambda_s + \lambda_b) \ln \frac{1 + \frac{\lambda_b}{\lambda_s}}{M} \right] \text{ bits/sec} \quad (30)$$

The slot width limited region is approximated [16] as

$$C_0 = \frac{\log_2 M}{M T_s} (1 - e^{-M \lambda_s T_s}) \text{ bits/sec} \quad (31)$$

Here,  $\lambda_s = \frac{P_s \lambda}{hc}$  and  $\lambda_b = \frac{P_b \lambda}{hc}$

i.e. signal and background photons per second,  $P$  = Signal and background power, as appropriate,  $\lambda$  is the wavelength and  $T_s$  is the slot width. The algorithm that the receiver module uses takes the signal and background noise levels and tries to optimize  $M$  to achieve the highest possible data rate. To start, the width of the time slot is fixed, as a fast as the laser transmitter can modulate data.  $M$  is assumed to be 2 to start, and then increased by a factor of 2 at a time until the data rate does not increase any more. The code is also subject to limits on peak laser power, so that infinitely high  $M$ 's are not possible.

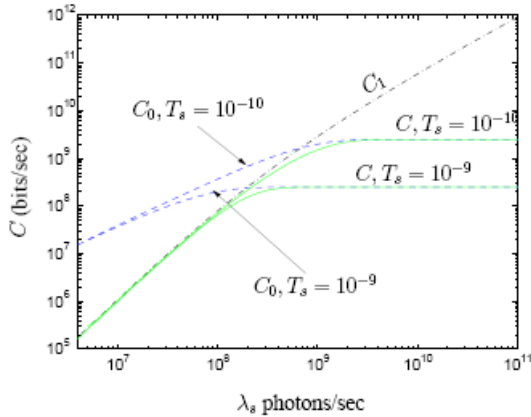


Figure 19 – Channel Capacity Calculation

This is tight over a broader region, and spans the transition region well. The channel capacity calculated for a hypothetical case is shown in Figure 25 (bottom) to illustrate the effect on background noise levels on the noise dominated region. Channel Capacities for varying  $M$  are shown in Figure 25 (main graphic), and match with JPL's version. Bit error rates are corrected using error correcting codes whose rate is given by:

$$R = C M T_s / \log_2(M) \quad (32)$$

As the signal photon levels change,  $M$  adjusts automatically causing jumps in the channel capacity as demonstrated in the JPL simulation as well. Signal to noise ratio will be given as:

$$\text{[Redacted]} \quad (33)$$

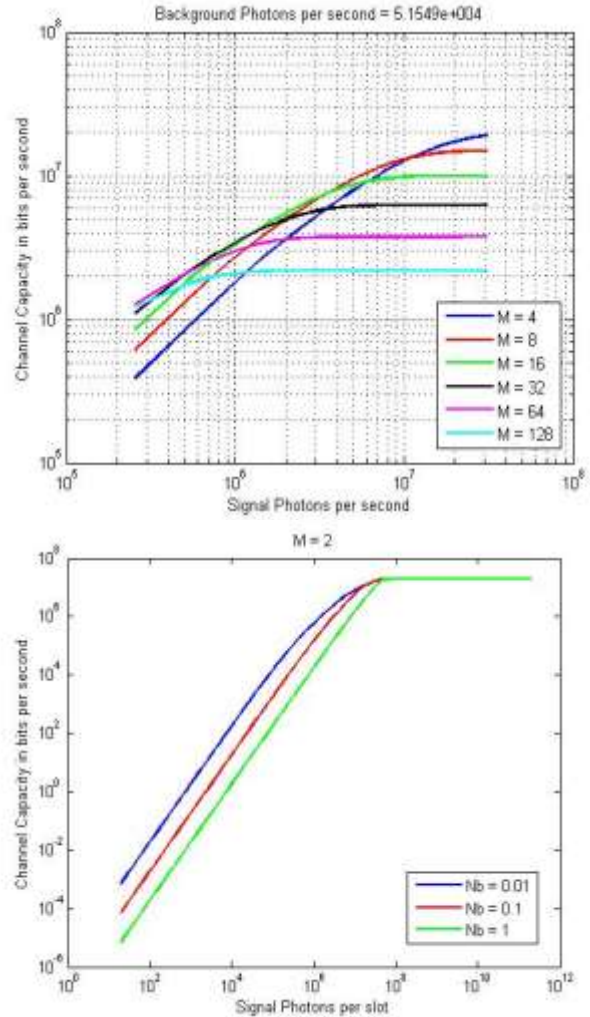


Figure 20 – Channel Capacity

### Acquisition, Tracking and Pointing (ATP)

**Gimbal Specifications**—To drive and control the pitch (elevation) and yaw (azimuth) of the laser device, a two axis gimbal (mounted on the Hopper) will direct the laser beam to hit the laser receiver on the Earth; gimbal accuracy and precision need to be determined. The PTU-D46-70 gimbal [17] made by Directed Perception in Burlingame, CA, needs to be evaluated. This gimbal was selected by Sierra Nevada for use in the Next Giant Leap team hopper, and is anticipated to be the mount for the laser communications payload. The PTU-D46-70 is expected to have a position resolution of 0.0032° per 1/8 step of motion. Custom range

extension would allow us to meet any pointing range requirements. Individual units have been space-qualified and flown on a space shuttle mission. The PTU-D46-70 is a COTS computer-controlled pan-tilt gimbal. It is small in size (5.16''x2.525'') and features a pointing resolution of 0.0032° at 1/8 step or 0.013° at 1/2 step.

Performance of the unit is summarized in the table below.

Max Payload Weight (nominal)	9 lbs.
Position Resolution (°)	0.013 (1/2 step), 0.0032 (1/8 step)
Min Pan Speed	0.0032 °/sec
Max Pan Speed	60 °/sec
Min Tilt Speed	0.0032 °/ sec
Max tilt Speed	60 °/sec
Pan Range	+/- 180 °C
Tilt Range	+ 31/ -80 °C
Weight	3 lbs. (gimbal), 8 oz. (controller)
Height	5.2 in
Operating voltage	9-30 VDC
Environmental	IP65 (with weatherization option)
Operating Temperature	-20 ° C to +60 ° C
Power	9-30 V DC

**Table 4–Summarized Gimbal specification (PTU-D46-70)**

Accuracy and Precision: Lincoln previously stated requirements for accuracy and precision are 500 μrad and 100 μrad respectively, which translates to 0.028 and 0.006 degrees respectively. Gimbal manufacturer does not provide figures for the accuracy of the PTU-D46-70 by this definition. Therefore, it is necessary to determine this experimentally.

Load Capacity: The unit can support a load of 9 lbs (about 4kg). The communication system of the hopper is listed as 14 kg margined on the MEL, but the mass of an RF antenna alone is significantly less. This will leave at least 1.5 kg for the laser system, which should be sufficient for the laser (non-electronics) components.

Range of Motion: The tilt range of the gimbal is -47° to +31° from level and the pan range is +/- 159°. There is a possibility of a range extender which would allow 80° down tilt and +/- 180° for pan or more. The range can be extended to meet the needs according to a Directed Perception. If hopper lands near the equator of the moon, the extended range may not be required. The penalty of extending the range is that 1/8<sup>th</sup> stepping no longer works.

*Target Specifications*—The STARFIRE Optical Range located in Albuquerque, NM (Latitude: 35.0845°, Longitude: - 106.651°) has been selected by the Laser Team as first choice for a receiver because it has high receiver aperture (1.5 and 3.5 meters), low weather and high accessibility (AFRL owned and operated). All STK calculations are based on STARFIRE location (Second

choice is APOLLO located in Apache Point, NM, 3.5 meter aperture, low weather variability, NMSU owned and operated; and third choice is FIREPOND located in Westford, MA, 1.2 meter aperture, high weather variability, and MIT Lincoln Lab owned and operated)

*Acquisition, Tracking, and Pointing (ATP) Theory*—The off axis intensity of a Gaussian beam on a plane at a distance of z from the source, at a distance of r from the centre of the plane, when the source emits a power of P is given by [18]:

$$I(r, z) = \frac{2P}{\pi w^2(z)} \exp\left(-\frac{2r^2}{w^2(z)}\right)$$

$$w(z) = w_0 \sqrt{1 + \frac{z^2}{z_R^2}}$$

$$z_R = \frac{\pi w_0^2}{\lambda}$$
(34)

From Figure 21, the circles represent the wave fronts of the laser beam intersecting an image plane (at a distance z from the source). The centre is the point of maximum intensity of the received Gaussian and the intensity falls off with radius (r) from the centre. Ideally, the receiver to be at this central point, however due to pointing errors, it may be at a random distance away from the centre as shown. In this case, it collects the intensity I(r,z) of the beam given by Equation (34) instead of maximum intensity.

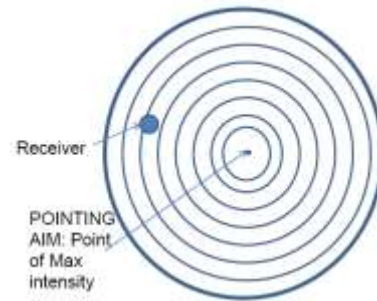


**Figure 21**

The rate at which Intensity falls off is given by [19]:

$$\frac{dI}{d\theta} = -\frac{I}{\sigma^2} \theta \quad \frac{dI}{dr} = -\frac{I\theta}{\sigma^2 L}$$
(35)

If the value of dI/dr for the receiver radii of <3 m is very low, the power received at the receiver at an off-axis distance of r on the image plane will be given as:

$$P(x, z) = \frac{2P}{\pi w^2(z)} \exp\left(-\frac{2\theta^2 L^2}{w^2(z)}\right) \pi D_r^2$$
(36)

Thus, for an off axes point, with the approximation of a small receiver in comparison to the beam footprint, the power received gets scaled down by a factor of:

$$\text{Fraction\_MaxPower} = \exp\left(-\frac{2\theta^2 L^2}{w^2(z)}\right) \quad (37)$$

The variation of Intensity with transmitter diameter for various off-axis angles is considered in

Figure 22 for an approximate apogee distance of 400,000km and Transmitting power of 200 mW. As shown in earlier discussions, the beam footprint size varies very insignificantly with perigee apogee distance so for the design tradespaces an average value is assumed.

Figure 22 and Figure 23 make it clear that larger transmitter diameter imply tighter beam and thus smaller spot sizes on Earth. So, although at no pointing error, the maximum intensity of a small spot sized beam will be much more than that of a larger beam – BUT for the same finite pointing error, larger transmitter diameter implies the danger of intensity falling off too quickly i.e. less power received at an off-axis point.

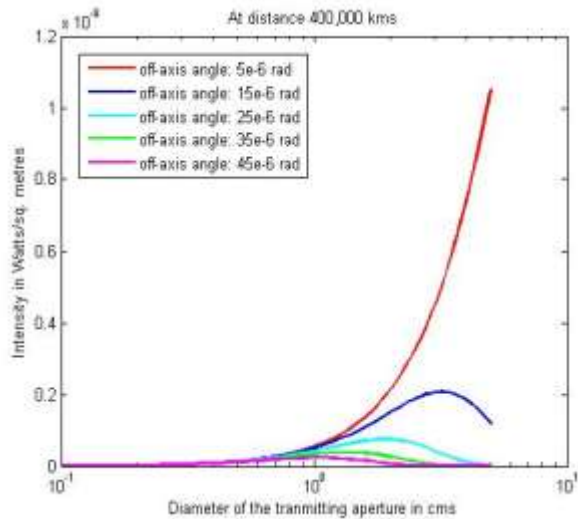


**Figure 22 – Intensity variation with transmitter aperture**

Pointing means orienting the laser device from the Moon to a laser receiver on the Earth which has a specific geographic position on inertial direction. A budget for pointing errors needs to be developed to know how much these errors contribute to the overall pointing accuracy. This accuracy budget drives both the cost and performance of a space mission. Basic pointing errors are associated with spacecraft navigation that is, knowledge of its position and attitude in space. But even if the position and attitude are known precisely, a number of other errors will be present. For example, an error in the observation time will result in an error in the computed location of the laser receiver because the laser receiver frame of reference moves relative to the laser device. The laser device mounting error represents the misalignment between the laser device and the sensors used to determine the attitude; this error is extremely difficult to remove. Because it cannot be determined from the attitude

data alone, it must be taken care as a critical parameter and keep it small while integrating the hopper.

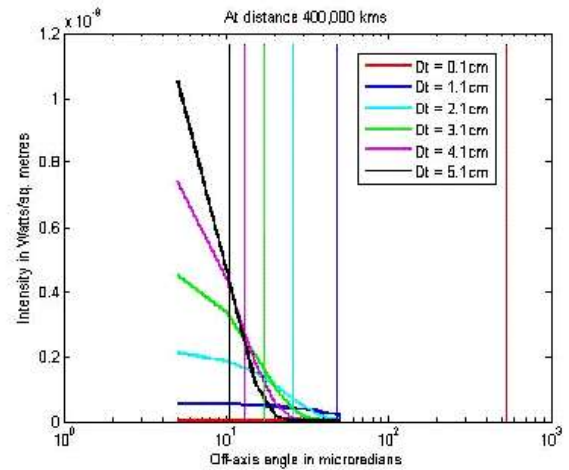


**Figure 23 – Intensity variation with off axis angle**

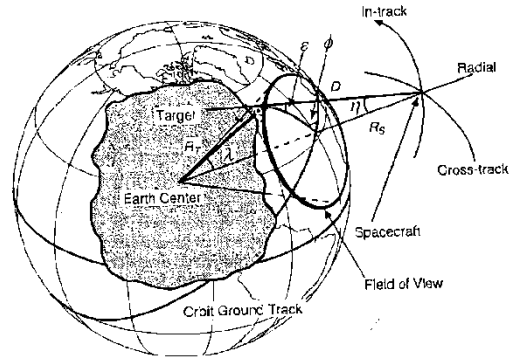


**Figure 24 – Definition of Pointing Error Components**

Because the laser device will transmit only when hopper is on a fixed point on the surface of the moon, the source of pointing errors are reduced considerably to Sensing Axis Orientation Errors that include the Hopper attitude determination based on its position on the Moon respect to the Receiver on the Earth, the instrument mounting (overall jitter), and control for pointing (see Table 5). A recent pointing design for a deep-space communications link (JPL accomplished projects [2]) set the total pointing loss allocation at 2 dB. To keep mispoint losses low (< 2 dB), the required pointing accuracy of the transmit signal is generally less than 40% of the diffraction-limited beamwidth. Table 6 has the data rate values for different transmitter aperture sizes (first two are reference examples of accomplished mission reference: Mars-to-Earth and Europa Orbiter-to-Earth) calculated for 2dB and 3dB pointing loss. To design the ATP system for the “Lasercomm Project” (Moon-to-Earth), allocations need to be made to determine the total mispoint angle caused by jitter and bias errors depending on the considered components like platform micro-vibration spectrum, and the particular link scenario like range, dead-banding, and noise

background sources. The value is limited by what the system components can perform, but it sets a preference upon which to set the requirements for jitter and bias errors.

The main sources of error are pointing knowledge jitter, residual tracking jitter, knowledge bias, and misalignment bias due to thermal/mechanical effects. A reasonable allocation of the total mispoint angle partitions divides into four parts and distributes it into one part for bias and three parts for jitter, as shown in Table 6. But, this initial apportioning serves as a guide to set the initial requirements that the subsystems would need to meet in order to support high rate optical communication links. This allocation can be later refined once estimates of the separate components are obtained.

HOPPER POSITION ERROR:			
1	$\Delta I$	In- or along-track	Displacement along the hopper's velocity vector
2	$\Delta C$	Cross-track	Displacement normal to the hopper's orbit plane
3	$\Delta R_s$	Radial	Displacement toward the center of the Earth (nadir)
SENSING AXIS ORIENTATION ERRORS (in polar coordinates about nadir) include: (1) attitude determination, (2) instrument mounting, and (3) control for pointing			
4	$\Delta \phi$	Azimuth	Error in rotation of the sensing axis about nadir
5	$\Delta \eta$	Elevation	Error in angle from nadir to sensing axis
OTHER ERRORS:			
6	$\Delta R_T$	Target altitude	Uncertainty in the altitude of the observed
7	$\Delta T$	Clock error	Uncertainty in the real observation time (result in uncertainty in the rotational position of the Earth)

**Table 5 – Sources of Pointing Errors**

*Pointing Error Budget Allocations<sup>3</sup>*

The major sources of jitter error are the pointing knowledge jitter error (knowing the position of the receiver) and the residual tracking error, which is the amount of vibration not compensated by the tracking loop. The major sources of the bias error are the bias in knowledge of the receiver position and the bias caused by mechanical and thermal effects. The sources of the static pointing error include algorithm error, the error in estimating the Earth-receiver position, the ephemeris error, error in computing the point-ahead angle, and alignment errors.

The boresight alignment error and errors due to thermal-mechanical distortion are considerable sources of static errors; these sources can be controlled with careful opto-mechanical design and with careful alignment of the optics.

Internally Generated Disturbances and Residual Errors are explained below.

Noise Equivalent Angle (NEA): A contributor of noise which is internally generated includes the receiver NEA (only when an uplink is going to be used for tracking and

pointing). This is a measure of the angular jitter in the tracking system that results from the detection process.

Total mispoint angle, $\beta$ ( $\mu$ rad)	0.921	1.534	4.469	8.938	44.69	89.38
Tx aperture, D, (m)	0.5	0.3	0.1	0.05	0.01	0.005
Total pointing jitter error ( $\mu$ rad)	0.231	0.383	1.12	2.23	11.17	22.35
Pointing knowledge jitter	0.163	0.271	0.79	1.58	7.91	15.82
Residual tracking knowledge	0.163	0.271	0.79	1.58	7.91	15.82
Total pointing bias error ( $\mu$ rad)	0.231	0.383	1.12	2.23	11.17	22.35
Pointing knowledge bias	0.163	0.271	0.79	1.58	7.91	15.82
Mechanical, thermal	0.163	0.271	0.79	1.58	7.91	15.82

**Table 6 – ATP Total Pointing Error**

The NEA is a function of the received spot image size, the received spot spatial intensity profile, and the received SNR (*Signal to Noise Ratio*) in the tracking bandwidth.

The NEA, or  $\sigma_{rms}$ , is calculated by:

$$\sigma_{rms} = \frac{1}{SF \sqrt{SNR}}$$

Where, SF (slope factor) is defined as the transfer function through the origin and converts the angular offset to a linear voltage; SF is expressed in units per radian and  $\theta_A$  is the optical spot diameter in radians.

$$SF = \frac{4.14}{\theta_A} \quad SF = \frac{1.56}{\theta_A} \quad SF = \frac{1.27}{\theta_A}$$

For Airy pattern intensity profile

For Gaussian spot intensity profile

For Uniform spot intensity profile

Residual jitter is associated with the gimbal system, which cannot be tracked out by the fast steering mirrors. The pointing jitter error represents 3/4 of the total system pointing error, leaving 1/4 for the pointing bias error.

One critical aspect of laser communication with narrow beams results from the need to introduce a point-ahead angle that is used to compensate for the time of travel of the light,  $c = 299,792,458$  m/s, over the long cross ranges. Because of the finite velocity of light and the relative angular velocity of two communication terminals moving in space, the transmit beam must be directed towards the receiver's position it will have at some time later. At the distance  $D_{LT}$  (Laser to Target), the round trip light time is  $2D_{LT}/c$ , where  $c$  is the speed of light. The point ahead angle (at inferior conjunction,  $180^\circ$  phase angle) is independent of the distance  $D_{LT}$ , and it is given by:

$$Point\text{-ahead angle} = \frac{2D_{LT} * target\ projected\ velocity}{c D_{LT}}$$

$$Point\text{-ahead angle} = \frac{2 * target\ projected\ velocity}{c} ; (rad)$$

Mission	Data Rate (Mb/s)	Range (AU)	Tx aperture (m)	$\lambda$ Down-link (nm)	$P_{TX}$ (W)	Pointing Loss, $L_{\beta}$ (dB)	Pointing Error, $\beta$ ( $\mu$ rad)	Jitter Error ( $\mu$ rad)	Bias Error ( $\mu$ rad)	Pointing Accuracy Radius, $r_{\beta}$ (km)	Divergence Angle, $\theta$ , ( $\mu$ rad)	Footprint Radius, $R_{MAX}$ (km)
Mars-to-Earth	40	2.7	0.30	1064	5	2	1.5	1.12	0.37	300.8	4.52	911.989
Europa Orbiter-to-Earth	0.4	6.4	0.30	1064	3	2	1.5	1.12	0.37	713.1	4.52	2161.752
Moon-to-Earth (at Moon's Apogee)	0.056 0.036	0.002 7	0.001	1064	0.3	2 3	446.88 545.30	335.16 408.98	111.72 136.32	90.403 110.313	1354.73	274.059
	5.69 3.84	0.002 7	0.0035	1064	0.3	2 3	127.68 155.80	95.76 116.85	31.92 38.95	25.829 31.518	387.06	78.303
	9.95 7.59	0.002 7	0.005	1064	0.3	2 3	89.38 109.06	67.03 81.79	22.35 27.27	18.081 22.063	270.95	54.812
	19.89 19.68	0.002 7	0.01	1064	0.3	2 3	44.69 54.53	33.52 40.89	11.17 13.64	9.040 11.031	135.47	27.406
	20.00 20.00	0.002 7	0.02	1064	0.3	2 3	22.34 27.27	16.76 20.45	5.58 6.82	4.520 5.516	67.74	13.703
	20.00 20.00	0.002 7	0.03	1064	0.3	2 3	14.90 18.18	11.17 13.63	3.73 4.55	3.013 3.677	45.16	9.135
	20.00 20.00	0.002 7	0.04	1064	0.3	2 3	11.17 13.63	8.38 10.22	2.79 3.41	2.260 2.758	33.87	6.851
	20.00 20.00	0.002 7	0.05	1064	0.3	2 3	8.94 10.91	6.70 8.18	2.24 2.73	1.808 2.206	27.09	5.481
	20.00 20.00	0.002 7	0.10	1064	0.3	2 3	4.47 5.45	3.35 4.09	1.12 1.36	0.904 1.103	13.55	2.741
	20.00 20.00	0.002 7	0.20	1064	0.3	2 3	2.23 2.73	1.68 2.05	0.55 0.68	0.452 0.552	6.77	1.370
	20.00 20.00	0.002 7	0.30	1064	0.3	2 3	1.49 1.82	1.12 1.36	0.37 0.46	0.301 0.368	4.52	0.914
	20.00 20.00	0.002 7	0.50	1064	0.3	2 3	0.894 1.091	0.670 0.818	0.224 0.273	0.181 0.276	2.71	0.548
	20.00 20.00	0.002 7	1.0	1064	0.3	2 3	0.447 0.545	0.335 0.409	0.112 0.136	0.090 0.110	1.35	0.274
	20.00 20.00	0.002 7	2.0	1064	0.3	2 3	0.223 0.273	0.167 0.205	0.056 0.068	0.045 0.055	0.68	0.137

Table 7 – Pointing loss, pointing error and pointing accuracy

The Laser Receiver is predicted to be located at NM (Starfire Optical Range latitude: 35.0845°) which has a projected velocity of 380.59 (m/s), so:

$$\text{Point-ahead angle} = \frac{2 * 380.59 (m/s)}{299,792,458 (m/s)}$$

$$\text{Point-ahead angle} = 2.539 \mu\text{rad}$$

The pointing system is usually commanded by the laser communication system’s pointing and tracking controller; feedback of the angular position of the pointing elements has some residual NEA just like the tracking system; these errors are typically small and very low frequency since pointing system typically is only compensating for point-ahead errors and alignment offsets.

The final error in the pointing system results from the alignment offsets of the transmit and receive paths. In many laser communication system designs, the tracking detector boresight is considered the system boresight; all other alignments are referenced to it. During manufacture and build-up of the optical system, the transmit and boresights should be mechanically aligned as precisely as possible to less than one tenth of the beam divergence ( $\theta/10$ ). Externally generated errors are also accounted for.

### 3 MODEL RESULTS

There are several multi-dimensional trade spaces that can be considered to produce the highest possible performance (data rate) within the constraints of the equipment capabilities and the environment. There are other significant constraints such as cost, and available power but these constraints are currently outside the scope of this study. Each trade space figure was made by assuming the nominal values in

Table 8, then varying two of the variables within their desired ranges. When three or more variables needed to be varied, separate figures were used or contours for each value of the 3<sup>rd</sup> variable were plotted on top of each other in the same figure.

Transmitted Power	300 mW
Transmitter Diameter (Aperture)	.0035 m
Receiver Diameter	1.5 m
Receiver Field of View	30 $\mu\text{rad}$
Range	378000 km
Pointing Error Loss	3 dB
Lunar Phase Angle	45 degrees (Average Lunar Background Noise)

**Table 8 – Nominal (Baseline) Trade Space Values**

The first trade space in Figure 25, Figure 26, and Figure 27 shows the data rate as a function of the power transmitted, the transmitter diameter, and lunar phase angle. The power

transmitted is a performance variable of the laser sub system but it is treated here as an independent variable to understand the implications of decreasing it and increasing it in the system requirements. The half power beam widths (HPBW) are shown in white dotted contours at equal intervals to show their exponential relationship with transmitter diameter. The three figures are for different lunar phase angles, 5 degrees, 45 degrees, and 90 degrees.

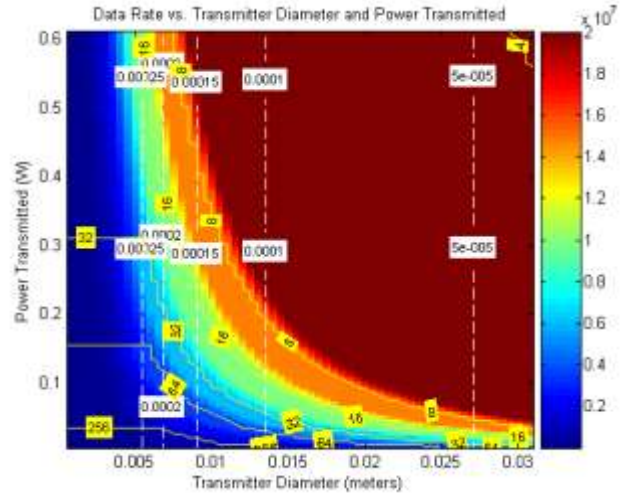


**Figure 25 – Bright Lunar Background (5 deg lunar phase angle). Yellow dotted lines denote the M-ary PPM’s ‘M’ and white dotted lines denote the HPBW value.**

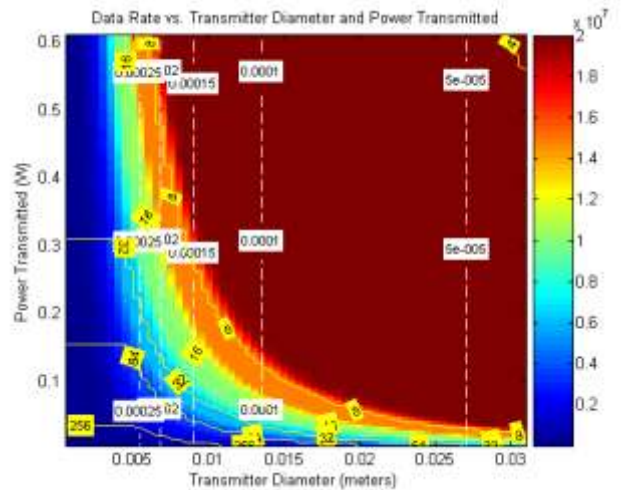


**Figure 26 – Average Lunar Background (45 deg lunar phase angle). Yellow dotted lines denote the M-ary PPM’s ‘M’ and white dotted lines denote the HPBW value.**

The moon contributes the most background noise at 5 degrees because the sun is “illuminating” the moon. The moon contributes the least amount of background noise at 90 degrees because the sun’s illumination effect is pointed away from the earth. M-ary PPM is shown in yellow. The

Matlab code dynamically selects the optimal M-ary PPM to maximize data rate.

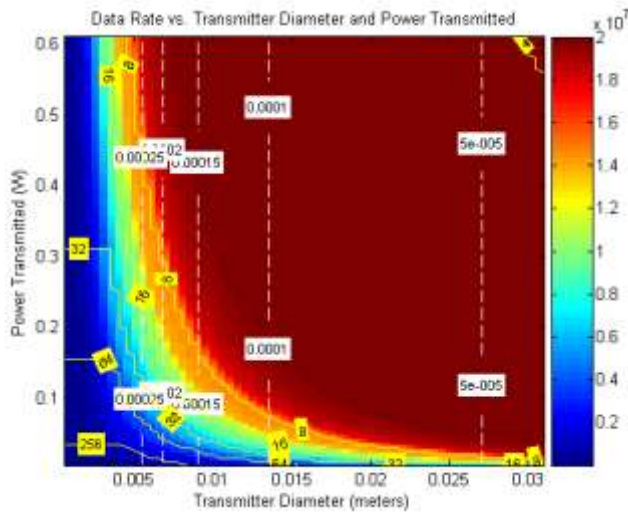


**Figure 27–Weak Lunar Background (90 deg lunar phase angle). Yellow dotted lines denote the M-ary PPM’s ‘M’ and white dotted lines denote the HPBW value.**

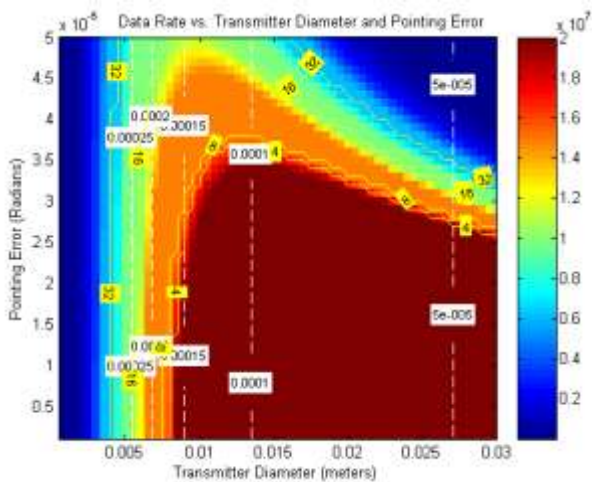


**Figure 28 – Pointer Error Effects (Weak Lunar Background). Yellow dotted lines denote the M-ary PPM’s ‘M’ and white dotted lines denote the HPBW value.**

The objective of this specific trade space is to maximize the data rate within the equipment limits and understand how compromises that maintain performance can be made. The current equipment limit is the gimbal pointing limit. The maximum useful half power beam width is limited by the minimum step change of the gimbal or the gimbal resolution of 25  $\mu$ rad. When the half power beamwidth becomes smaller than the gimbal pointing limit, the system enters the unfeasible region. It is deemed unfeasible because if the half power beam width is smaller than the gimbal resolution, there is no guarantee that the signal will be detected by the ground receiver. However these plots have been constrained such that only the feasible reason (HPBW > 25 $\mu$ rad) is shown. The trade space shows that a smaller

half power beam width leads to a higher data rate which physically corresponds to concentrating more signal strength over a smaller area instead of spreading out the strength over a larger area. There is a saturated region (reddish maroon) at 20 Mb/s. This region is well above the Lincoln performance target of 1 - 2 Mb/s.

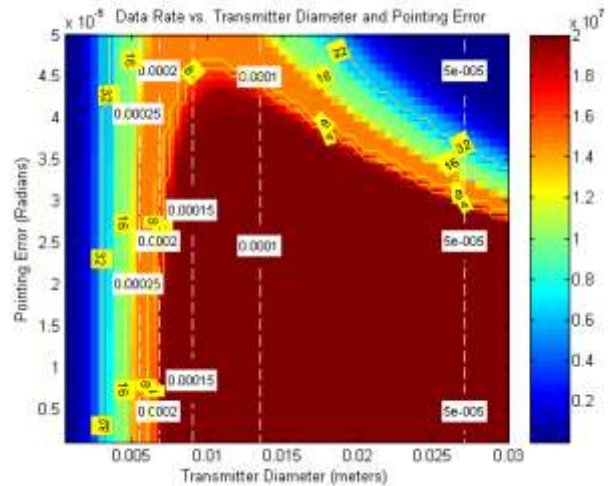


**Figure 29 – Pointer Error Effects (Average Lunar Background)**

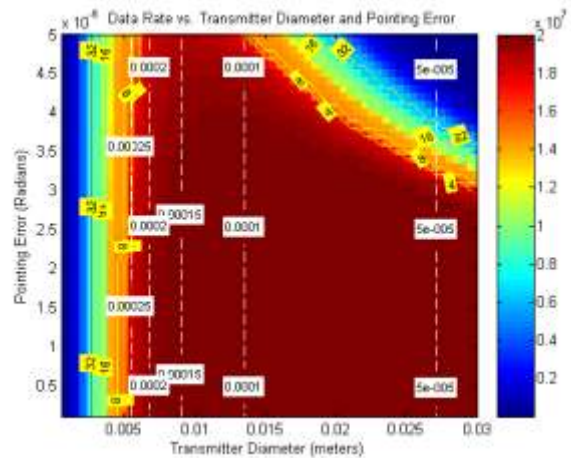
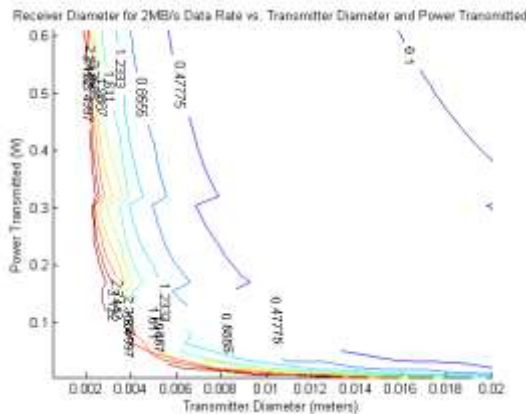


**Figure 30 – Pointer Error Effects (Bright Lunar Background)**

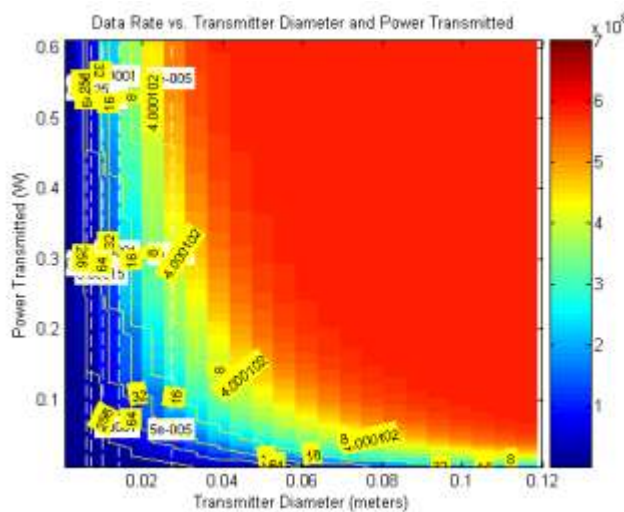
The Receiver Field of View is a key design variable that can directly enhance the quality of the signal received by the detector and thus the data rate if set to the lowest possible working value. Decreasing the field of view effectively shields the receiver from unwanted background noise from the moon while focusing more finely on the optical signal from the laser. However, decreasing the field of view too much can be detrimental because the actual laser signal will partially be filtered out from reaching the receiver.

A signal to noise ratio between 30 and 40 million (given by Equation 32) is expected based on the current nominal values and equipment capabilities. This trade space can be used to provide insight into the technical impact of reducing

field of view when underperforming designs are proposed and validation when high performing designs are reached. Pointing error has an  $x^2$  relationship with transmitted power. As the power increases, the data rate increases. Pointing Error Effects show in Figure 28, Figure 29, and Figure 30 show a unique interaction between pointing error and transmitter diameter producing a near upside-down L shaped plot for data rate. As the pointing error increases, the data rate will decrease but varying the transmitter diameter has a competing effect of adding signal strength to the transmitted signal. The downward sloping, *decreasing*, data rate lines that follow an increased transmitter diameter *after* an increase in data rate are due to the narrower beam missing the transmitter. As the beam gets more powerful it becomes narrower with a higher peak. The negative effect of a more powerful beam is that outside of the main Airy disk, the beam strengths become weaker far more rapidly. Increasing the transmitter diameter effectively decreases the size of the main Airy disk, the width of the disk where the half peak power (or HPBW) occurs, and results in a weaker signal at the same distance from the center. The vertical white lines show the corresponding half power beam width. The reddish-maroon region shows where the saturation occurs at a data rate of 2mb per second.



To compare and validate the model results, the input values for the Laddee spacecraft were used. The Laddee spacecraft is a lunar orbiting spacecraft capable of 600 Mb/s data rates. The Laddee is a suitable case study because it uses the same optical transmission technology that is proposed by Lincoln Laboratory for the Lunar X-Prize but with higher performance and a higher cost. In order to remove the current saturation of data rate at 20 Mb/s, the limit on minimum time slot (25 nanoseconds) was reduced until the 600 Mb/s data rate was reached. In Figure 35, a time slot of 0.82 nanoseconds was used to achieve data rate 610 Mb/s on the saturation contour. The time slot of 0.82 nanoseconds was feasible to receive, the model predicts that the data rate of 600 Mb/s for the Laddee specifications (1m Transmitter diameter and 500 mW of transmitted power), would be possible.



- [11] D. L. Walters, Atmospheric modulation transfer function for desert and mountain locations:  $r_0$  measurements, *J. Opt. Soc. Am.*/Vol. 71, No. 4/April 1981.
- [12] P. I. Hopman et al, An End-to-End Demonstration of a Receiver Array Based Free-Space Photon Counting Communications Link, *Proc. of SPIE* Vol. 6304, 63040H, 2006.
- [13] D. L. Walters and L. W. Bradford, "Measurements of  $r_0$  : Two Decades and 18 Sites, *Applied Optics*, vol. 36, pp. 7876–7886, 1997.
- [14] H. Kieffer, T. Stone, The Spectral Irradiance of the Moon, *The Astronomical Journal*, 129:2887-2901, June 2005.
- [15] M. Charbit, C. Bendjaballah, Efficient capacity for a PPM weak noisy photon-counting channel, *Optical and Quantum Electronics*, Volume 18, Number 1, 49-55, DOI: 10.1007/BF02069360, 1986.
- [16] B. Moision and J. Hamkins, Deep-Space Optical Communications Downlink Budget: Modulation and Coding, *IBN Progress Reports* 2003.
- [17] Emilly B Gross, Lincoln Laboratory doc EBG.001.09-MEM, PTU-D46-70 Gimbal Report, 2009.
- [18] Tobias Schmitt-Manderbach, Long distance free-space quantum key distribution, Dissertation at the Faculty of Physics of the Ludwig-Maximilians-Universität München, 2007.
- [19] C.W. Hindman, B.S. Engberg, Atmospheric and Platform Jitter Effects on Laser Acquisition Patterns, *IEEE Aerospace Conference* 2006.

## 7 BIOGRAPHY



Sreeja Nag is a graduate research assistant in the Space Systems Laboratory (SSL) at the Massachusetts Institute of Technology and leads the SPHERES Zero Robotics Program. She is a dual SM Candidate in Aeronautics & Astronautics Engineering along with Technology & Policy at MIT. She

has summer research experience with NASA JPL in 2008 and the European Space Agency (ESTEC) in 2010. Prior to joining SSL, she was working on the DARPA F6 program on Fractionated Spacecrafts.

Email: [sreeja\\_n@mit.edu](mailto:sreeja_n@mit.edu)



Edwin Gomez is a graduate student in the MIT Advanced Study Program (ASP) with concentration in Aeronautics and Astronautics. His research interests include space systems engineering, satellite engineering design, space propulsion, and systems safety. He

works for Raytheon BBN Technologies as Hardware Test Engineer in the Boomerang Project since 2008. Prior Raytheon, he was working as Avionics and Electrical Systems Engineer for Gulfstream Aerospace Corporation in Savannah, Georgia. Edwin has been serving in the US Army since 2005 and he is a senior member of the American Institute of Aeronautics and Astronautics and a member of the IEEE Aerospace and Electronic Systems Society.

Email: [ergomez@mit.edu](mailto:ergomez@mit.edu)



Sam Feller is an employee at MIT Lincoln Laboratory. He graduated in 2007 with a BS in Mechanical Engineering from WPI. His interests include systems engineering, control systems, and design of precision mechanisms, and robotics. He also volunteers as a high school lacrosse coach in his free time.

E-mail: [samuel.feller@ll.mit.edu](mailto:samuel.feller@ll.mit.edu)



Jonathan Gibbs is a graduate research assistant in the Center for Aerospace Policy Research (CASPOR) working on risk assessment frameworks and an SM Candidate in the Department of Aeronautics and Astronautics.

He has previously worked for the Boeing Company, and completed his S.B. at MIT in 2006 in

Aeronautics and Astronautics.

Email: [jaygibbs@mit.edu](mailto:jaygibbs@mit.edu)



Dr. Jeffrey Hoffman is currently the director of the Massachusetts Space Grant Consortium and an MIT Professor of the Practice of Aerospace Engineering, where he teaches courses on space operations, space systems design, and space policy. He is a former NASA astronaut who has made five space flights, becoming the

first astronaut to log 1000 hours of flight time aboard the Space Shuttle. Email: [jhoffman1@mit.edu](mailto:jhoffman1@mit.edu)